International Journal of Extreme Manufacturing

TOPICAL REVIEW • OPEN ACCESS

Meniscus fabrication of halide perovskite thin films at high throughput for large area and low-cost solar panels

To cite this article: Xuezeng Dai *et al* 2019 *Int. J. Extrem. Manuf.* **1** 022004

View the article online for updates and enhancements.

This content was downloaded from IP address 118.123.172.215 on 06/08/2019 at 12:29

OPEN ACCESS
IOP Publishing | IMMT
International Journal of Extreme Manufacturing
Int. J. Extrem. Manuf. 1 (2019) 022004 (14pp)
https://doi.org/10.1088/2631-7990/ab263e

Topical Review

Meniscus fabrication of halide perovskite thin films at high throughput for large area and low-cost solar panels

Xuezeng Dai, Yehao Deng, Charles H Van Brackle and Jinsong Huang[1]

Department of Applied Physical Sciences, University of North Carolina, Chapel Hill, NC 27599, United States of America

E-mail: jhuang@unc.edu

Received 16 May 2019
Accepted for publication 26 May 2019
Published 26 June 2019

Abstract

Halide perovskites have rapidly attracted considerable attention due to unprecedented properties not seen in traditional semiconductors. In addition to their optoelectronic merits, one advantage of perovskite materials is their solution processability, which opens the door to low-cost and high throughput solution coating strategies for the commercialization of perovskite solar cells (PSCs). Here we review perovskite film fabrication by meniscus coating—a simple and readily scalable manufacturing technique, including blade coating and slot-die coating. We outline the fundamental fluid mechanisms of meniscus coating, discuss drying and crystallization of perovskite in the coating process, and provide an overview of recent progress in meniscus-coated PSCs.

Keywords: meniscus coating, large area, perovskite thin films

(Some figures may appear in colour only in the online journal)

1. Introduction

As the technology rapidly advances and the costs reduce, the demand for solar panels continues to grow. Nearly 100 GW of grid-connected solar panels were installed in 2017, an almost 30% increase over the 77 GW added in 2016 [1]. Analysts predict that the world's photovoltaic (PV) production capacity could reach one terawatt by 2022 [1]. At the same time, various new markets are emerging for cost-efficient renewable power, such as portable power supplies, electric vehicles, and building-integrated PVs. The ever-decreasing price of solar energy plays an important role in promoting clean energy in these rapidly developing markets. The projected total system levelized cost of electricity (LCOE) of solar power is currently \$48.8/MWh, according to the US Energy Information Administration [2]. The estimated cost dropped 88% from 2010 to 2019. Many developments in the industry have contributed to that price reduction, but now it is new thin film PV technologies which are emerging with great promise to further reduce the cost of solar energy.

Halide perovskite solar cells (PSCs) is one such emerging PV technology. They have received considerable attention in recent years due to perovskite's intriguing optoelectronic properties including long charge diffusion length, high carrier mobility, and large absorption coefficient [3–7]. Because of these qualities—among others—the power conversion efficiency (PCE) of small, single-junction PSCs has rocketed to 24.2%, which is already the highest of all thin film PV technologies [8]. The high optical absorption coefficient of up to 10^4 cm^{-1} is a critical merit for commercialization; films of just 300–1000 nm are sufficient to collect the

[1] Author to whom any correspondence should be addressed.

Original content from this work may be used under the terms of the Creative Commons Attribution 3.0 licence. Any further distribution of this work must maintain attribution to the author(s) and the title of the work, journal citation and DOI.

© 2019 The Author(s). Published by IOP Publishing Ltd on behalf of the IMMT

Table 1. Commercialization of perovskite solar cells.

Company	Country	Fabrication method	Demonstrated best performance
Oxford PV	UK	Evaporation	28% PCE for 1 cm^2 perovskite-silicon tandem solar cells
Solaronix	Switzerland	Printing	12% PCE for 500 cm^2 modules[a]
Saule technologies	Poland	Inkjet printing	Custom patterned ink-jet printing
Solliance	Netherlands	Roll to roll slot-die coating	13.5% PCE for 0.09 cm^2 cells
Toshiba	Japan	Meniscus coating	11.7% PCE for 703 cm^2 modules[a]
Microquanta semiconductor	China	—	Certified 17.25% PCE for 17.277 cm^2 mini-modules

[a] Did not report whether PCE was calculated by aperture area or active area.

photons sufficient for achieving high efficiencies. Compared to inorganic thin film absorber layer thicknesses of around 3 μm, it not only reduces material use and processing costs but also enables high production throughput. Han *et al* calculated the manufacturing cost of perovskite modules [9], with estimates as low as $\$30/m^2$ to $\$41/m^2$ without considering panel components such as sealing the glass and junction box. The corresponding LCOE is quite low, only \$35-\$49/MWh with a module efficiency between 12% to 20% and a 15 year lifetime. However, to value the commercial product, the cost needs to consider the total panel system. Heben *et al* established a more comprehensive model which considered assembling the panel components. By using a printing strategy to fabricate the hole transport and electron transport layers (HTL and ETL, respectively), the production throughput can be 1.44 $m^2\,min^{-1}$. Thus, the annual capacity could reach 121 MW $year^{-1}$ with a module efficiency of 16%. The LCOE is in the range of \$49.3 to \$79.0/MWh assuming a system lifetime of 30 years [10].

To scale up and reduce manufacturing costs, effective mass production methods should be implemented to fabricate perovskite films. Several versatile film deposition methods have been reported to fabricate high-quality perovskite films for PV applications; these can be classified as a vapor deposition method (typically conducted by thermal evaporation) or a solution-based method in terms of the phase of precursor material used for manufacturing. For example, co-evaporation of PbI_2 and CH_3NH_3I (MAI) yields a uniform, compact perovskite layer on the substrate. However, this mode of film deposition faces significant challenges that limit the scale of film production. Tarasov and collaborators innovated a new vapor evaporation strategy by taking advantage of the redox reaction of reactive polyiodide melts and lead to form perovskite [11]. Thin film Pb and MAI were first deposited stoichiometrically on a substrate by thermal evaporation. The as-deposited film is then treated with I_2 vapor, converting the Pb/MAI bilayers into $MAPbI_3$. Devices fabricated by such strategy achieved PCE of 17.18% with the capability of making large films up to 600 cm^2. Another feature of the vapor method is that it can form a conformal thin film on textured substrates. Oxford PV exploits this merit to fabricate perovskite/silicon tandem solar cells, achieving 28% record PCE in 1 cm^2 (table 1) [12]. Although vapor deposition can form relatively large area films, it is not quite compatible with mass production due to sophisticated vacuum equipment and long processing times, reducing the final throughput. Due to these limitations, most of the institutes and companies are focusing on solution strategies to commercialize PSCs. Solution methods are well known, low-cost strategies that are capable of processing at low temperature under ambient conditions. Spin-coating is the widest-used solution method; almost all record efficiencies for PSCs are based on this method. However, spin-coating has very low throughput and wastes a large amount of precursor solution—not suitable for mass production. In contrast, other solution techniques like blade coating [13–16], slot-die coating [17–20], spray coating [21–23], and inkjet printing [24–26] are viable options for the scalable fabrication of perovskites. In industry, Solaronix and Saule Technologies have made efforts (shown in table 1) on printing strategies, which allow printing in custom patterns. Solaronix has achieved 12% PCE on modules with an area of 500 cm^2 [27]. However, whether they are suitable for large area mass production will depend on the printing speed and device structure [28]. Other companies have implemented meniscus coating, a simple coating method readily compatible with high throughput production. The term meniscus refers to the formation of the meniscus shape during coating of the solution. The meniscus configuration and fluid flows within it critically influence the morphology of the final solid film. Common meniscus coating methods include dip coating, blade coating, and slot-die coating. The Dutch firm Solliance demonstrated their roll-to-roll (R2R) slot-die coating capabilities, yielding large-scale perovskite production; their technique produced solar cells with a PCE as high as 13.5% for a device area of 0.09 cm^2 [19]. Toshiba produced the world's largest perovskite module: 702 cm^2–with a module efficiency of 11.7% [29]. The highest certified efficiency for a perovskite module in industry is a 17.25% PCE mini-module (17.3 cm^2) manufactured by Microquanta Semiconductor in China [30]. However, they did not report the film fabrication technique.

In this review, we summarize recent works implementing meniscus coating of perovskite films, because it is an efficient, low cost and high throughput film deposition technique that has been well established in many industries, though still relatively new for perovskites. An overview of the meniscus coating mechanism is described. The evolution of the perovskite from the initial wet meniscus to the solid, crystalline film is analyzed step-by-step. Works related to each phenomenon will be reviewed. Based on the fundamental understanding of the meniscus coating process, we provide perspectives on the development of the large area and low cost perovskite solar panels.

2. Basic configurations

2.1. Architecture of perovskite solar devices

Although this review does not fully cover the fabrication of each layer of perovskite devices, it is still worth considering the basic structures of cells and modules, because the interaction between the layers significantly impacts the deposition of perovskite films. For example, we demonstrated that spin-coating perovskite on non-wetting hole transport layers could increase nucleus spacing which facilitates the formation of perovskite films with large grains [31].

2.1.1. Structure of PSCs. Perovskite PVs are generally constructed with a thin film perovskite layer sandwiched between a p-type HTL and an n-type ETL. An n-i-p device structure with mesoporous metal oxide ETL was the first architecture of PSCs, following from dye-sensitized solar cells. Recently, a certified efficiency of 22.7% has been achieved based on this structure [32]. On the other hand, planar n-i-p and p-i-n structure without the mesoporous layer have proven to be efficient architectures as well. The highest reported efficiency of planar PSCs is 23.3%, with the aid surface passivation [33]. The planar architecture has excellent potential for low-cost mass production, due to its simple structure and circumvention of a high-temperature annealing process for the mesoporous metal oxide.

2.1.2. Architecture of perovskite solar modules. Solar modules constitute the PV panels that generate solar electricity for commercial use. Numerous individual, interconnected PV cells comprise each module. There are two interconnection architectures for modules. A simple way is called singulated interconnection, which is widely used in crystalline silicon (c-Si) solar modules. Single solar cells grown independently are then interconnected by external circuits to create modules. Unfortunately, this strategy of external connection creates a relatively large dead area which does not contribute to power production. On the other hand, perovskite solar modules, taking advantage of their continuous, large area coating capability, are more suitable for monolithic interconnection, where cells are defined by scribing through specific layers during the fabrication process, as shown in figures 1(d) and (e). This approach eliminates the external metal ribbons and reduces the dead area density—a major cost benefit [34].

2.2. Meniscus coating strategies

Meniscus coating can be defined as the translation of a meniscus over the surface of a substrate as the solution is spread by the coating tool. The shape of the meniscus, solution flows within it, and the solvent drying speed during and after coating the meniscus dramatically impact the morphology of the final, solid film. Common meniscus coating methods include dip coating, blade coating, and slot-die coating. Blade coating and slot-die coating are the most promising and reproducible strategies for the scalable

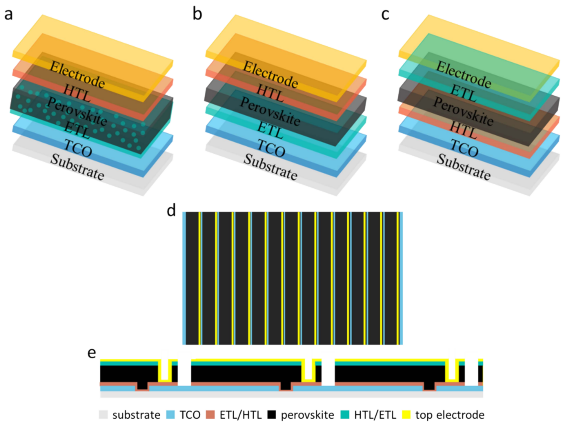

Figure 1. Architecture of perovskite solar devices. (a)–(c) Structure of perovskite solar cells. (a) Mesoporous n-i-p structure, (b) planar n-i-p structure, (c) planar p-i-n structure. (d), (e) Monolithically interconnected perovskite module; (d) plane view, (e) side view.

deposition of perovskite films; they are also amenable to roll-to-roll processing, which possesses great potential for manufacturing large area solar panels at high throughput for mass production.

2.2.1. Dip coating. Dip coating is a process that first immerses the substrate in the precursor solution and then lifts it out from the solution vertically with a specific velocity (figure 2(a)). A meniscus forms on the surface of the substrate at the interface between the precursor solution reservoir and the air (or inert atmosphere). Despite its simple appearance, complex interactions influence the film's structure and thickness, such as withdrawal speed, functionality of substrate surface, gravity, surface tension of solution, environmental temperature and humidity, as well as other factors [35]. In addition, the crystallization and phase transition of the perovskite will make the process far removed from handling. Also, the batch-to-batch immersion is a slow process that would hinder mass production. These drawbacks make dip coating an unpopular method for perovskite film fabrication.

2.2.2. Blade coating. Blade coating is one of the most versatile ways to spread the solution over a substrate. It is also known as 'doctor blading' or 'knife coating', because a doctor blade or knife is the primary instrument involved in the spreading process [36]. The coating solution is initially applied in the gap between a coating head and a substrate. Next, the blade travels across the substrate, spreading a uniform wet film and removing excess solution, as illustrated in figure 2(b). The wet film thickness can be related to the gap distance and also to the coating speed. Menisci form at both the advancing and receding sides of the blade. The advancing meniscus impacts the spread of solution onto the substrate which can limit the coating speed. Within the receding meniscus is a complex combination of different solution

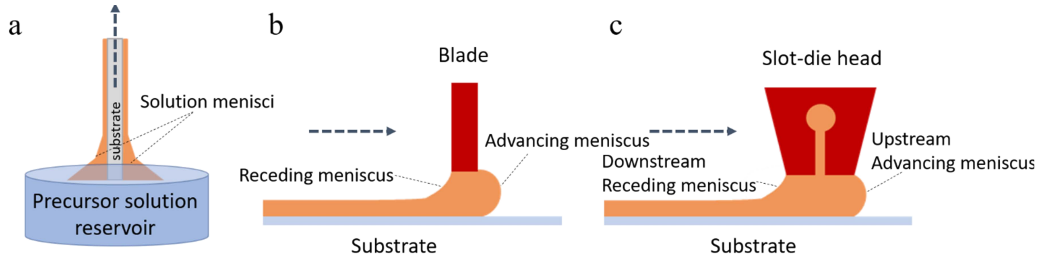

Figure 2. Schematic diagram of meniscus coatings. (a) Dip coating. (b) Blade coating. (c) Slot-die coating.

flows; this area largely determines film thickness and uniformity.

2.2.3. Slot-die coating. In slot-die coating, the coating solution is forced through a coating die onto the substrate as showing in figure 2(c). The coating die head, as well as the distributor in the system, consists of a distribution chamber and a feed slot which provides a uniform liquid flow rate over the entire coating width. The solution viscosity and capillary force dominant the film spreading. The coating gap underneath the downstream die is filled by solution whereas the upstream coating gap can be partially or completely filled [37]. Menisci form at both the upstream and downstream sides as in blade coating.

3. Meniscus coating processes and mechanisms

3.1. Advancing meniscus

The advancing, wetting meniscus is typically considered less than the receding meniscus since the latter is where the wet film forms and drying and solidification occur. However, the advancing meniscus is still valuable to study as it is the location of the first contact between the coating solution and substrate, and this wetting dynamic plays a vital role in limiting the coating speed.

Wetting is an essential process of coating—initially, coating head and substrate contact air. The precursor solution is injected, filling the room between the head and substrate. This spreading process is called static wetting, which also affects the coating process, though less directly. During coating, the liquid displaces air from the moving solid surface. The advancing meniscus obeys the rules of dynamic wetting. A straight and steady wetting line is crucial for uniform coating. Many theories have been established to describe static and dynamic wetting [38–40].

For static wetting under ideal conditions, smooth and chemically homogenous solids, and pure liquids, the thermodynamic equilibrium of gas, liquid and solid phases determine the unique static contact angle θ at which the liquid meniscus intersects the solid surface (figure 3(a)). According to Young's equation [41], the relationship between the contact angle θ, the solid–gas interfacial tension σ_{sg}, the solid–liquid interfacial tension σ_{sl}, and the liquid–gas interfacial tension σ_{lg} is:

$$\sigma_{sg} - \sigma_{sl} - \sigma_{lg}\cos(\theta) = 0.$$

If the vector sum of surface tension σ_{sg}, σ_{sl}, and σ_{lg} on the solid surface has the same direction as the solid–gas tension, then the liquid can spread on the solid spontaneously to form a film. The Wenzel [42] and Cassie [43] equations, which are the modification of Young's equation for heterogeneous substrates, are also well used to solve the wettability of the solid surface.

In the coating process, a wetting line moves with respect to the solid surface. The dynamic pressure and surface tension modulate the advancing meniscus of the wetting line. Dynamic wetting is usually characterized by the relative velocity of the wetting line and the dynamic contact angle between the dynamic liquid line and the solid surface. Dynamic wetting includes both spontaneous wetting and forced wetting. Forced wetting is the basic situation in meniscus coating, in which the contact line is driven by the external force of the coating head. Generally, the dynamic contact angle is velocity-dependent, which differs from its spontaneous wetting counterpart. As a consequence, dynamic wetting failure can be caused by an excessively high coating speed. The solution fails to form a continuous wet layer when the coating speed exceeds the critical speed U^{crit}, resulting in unsteady flows and air bubbles within the liquid [44]. Thus, manipulating dynamic wetting is one of the keys to high-speed coating. However, few studies have intensively investigated the high-speed coating of semiconductor materials, particularly perovskites.

3.2. Receding meniscus

Compared to the advancing meniscus, receding meniscus dynamics significantly influence the coated film quality. Various flows in the receding meniscus have been well investigated by researchers [45–47]. In the coating process, the coating head produces a shear force on the precursor solution filled in the space between head and substrate due to the relative movement. This shear force induces a shear-driven fluid motion called Couette flow [48] (figure 3(b)). The flow direction is parallel to the coating direction. Moreover, when considering the pressure gradient between the advancing and receding meniscus, the pressure differential can generate another force overlapping the shear force, tuning the flow magnitude and direction. A favorable pressure gradient in the direction of motion enhances the Couette flow. On the other hand, an adverse pressure gradient can weaken the

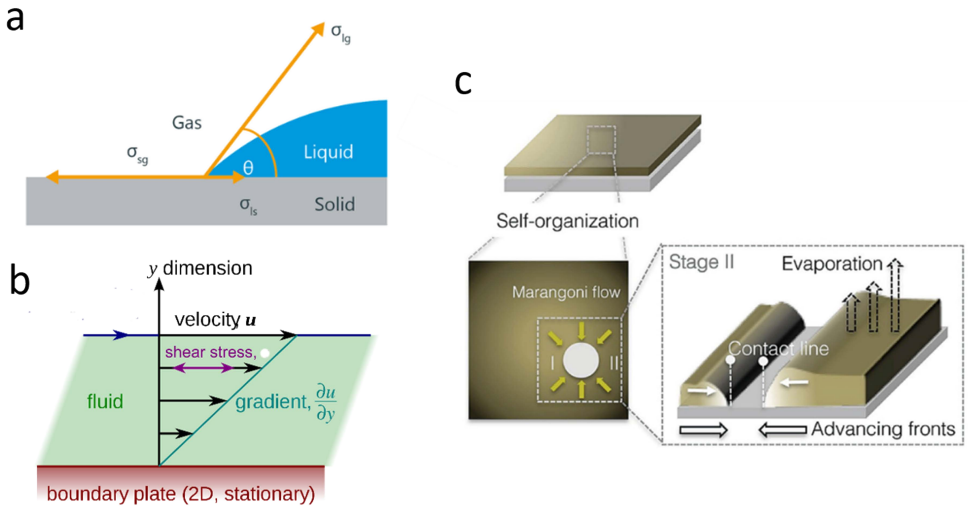

Figure 3. Mechanism of meniscus coating. (a) Schematic diagram of static wetting. (b) Schematic diagram of Couette flow. (c) Schematic diagram of Marangoni flow in spray coated perovskite film. (b) This 'Laminar shear in a fluid' image has been obtained by the author(s) from the Wikimedia website where it was made available 'Duk' under a CC BY-SA 3.0 licence. It is included within this article on that basis. It is attributed to 'Duk'. (c) [53] John Wiley & Sons. © 2016 WILEY-VCH Verlag GmbH & Co. KGaA, Weinheim.

Couette flow, even causing a reverse flow at the area far from the moving blade, where the shear force is weak.

Another primary flow is the Marangoni flow [49] triggered by the surface tension gradient along with the meniscus liquid-air interface (figure 3(c)). As the solvent evaporates, a higher concentration of solute near the solid film increases the surface tension, causing Marangoni flow toward the dry edge. Conversely, a reverse direction Marangoni flow can be induced by the thermal gradient from the dry edge to the bulk solution when heating the substrate during coating. Such a temperature gradient induced Marangoni flow can be characterized by the Marangoni number, a dimensionless number comparing the surface tension and viscous forces [50]

$$Ma = -\frac{d\gamma}{dT}\frac{\Delta TL}{\mu\alpha},$$

where γ is surface tension, T is temperature, L is effective length between the bar and substrate, μ is dynamic viscosity, and α is thermal diffusivity. Moreover, a faster evaporation rate close to the liquid-solid contact line induces the 'coffee ring' effect [51, 52]. A capillary flow can be created to equilibrate the fast solution losing at the edge.

Surface tension induced Marangoni flow is negligible in a single solvent system. However, solvent engineering of perovskite precursor solution usually involves mixed solvents, which can introduce surface tension gradients during evaporation, inducing Marangoni flow. Marangoni flow has been used to describe film formation in the spray coating of perovskite layers. It was regarded as the main mechanism of self-organization of gaps between spayed droplets. Tung *et al* [53] claimed the volatile difference of dimethyl sulfoxide (DMSO) and N-Methyl-2-Pyrrolidone (NMP) in solution leads to surface tension gradient from the edge to the center of each droplet. Therefore, driving force forms and spreads the droplets to mobilize the initially static pinning lines and recover the unwetted areas and pinholes, yielding compact films.

In addition, surfactants can also impact surface tension. When surfactant exists in solution, the energetic dynamics force the surfactant to reside at the free surface. As a result, the presence of surfactant at the surface reduces the surface energy. This surface tension gradient, in turn, causes Marangoni flow. We found such a mechanism can be used in blade coating perovskite to obtain large scale, uniform films [14]. *In situ* observation of the solution drying process immediately after blade coating shows that the intermediate phase solute moves to a crystalline perovskite island in 5 s. The solute flows toward the center of islands, leaving gaps between each island. To form compact perovskite layers, surfactants were introduced to the precursor solution. Consequently, the transportation of solute also carries the surfactants to the central island, creating a surfactant concentration gradient. The high concentration of surfactant in center reduced the surface tension, generating Marangoni flow in a direction reverse to original solute flow. Subsequently, the equilibrium of the two flows suppresses gaps between islands.

Meniscus flows can also induce alignment of coating materials when deposition speed falls in evaporation regime. Details will be described in the next section.

3.3. Coating regimes

Depending on the variation trend of solid film thickness, two coating speed regimes are identified in experimental results. In the low-speed regime, namely the evaporation regime, the drying timescale is comparable to moving speed. The solute accumulates and forms solid film right in the meniscus area (figure 4(a)). On the contrary, Landau–Levich regime is where coating speed is high enough so that wet films form and remain on the substrate due to the relatively low drying speed compared to the coating speed [54] (figure 4(b)).

These two deposition regimes were first combined to explain the thickness variation of blade coated phospholipid

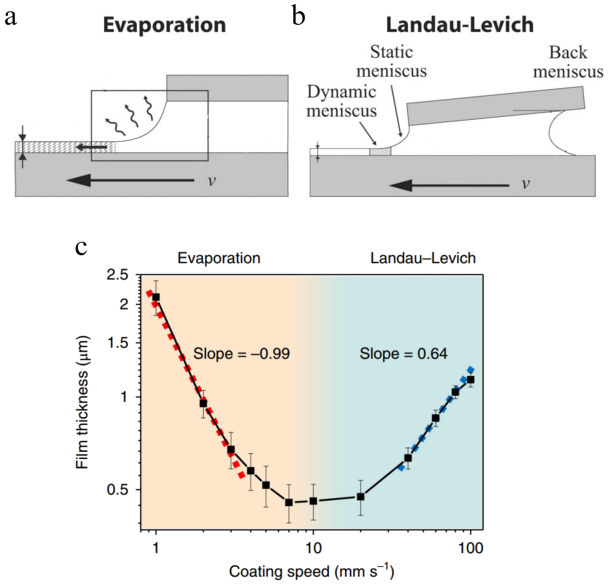

Figure 4. Meniscus coating regimes. (a), (b) Schematic of two deposition regimes. (a) Evaporation regime. (b) Landau–Levich regime. (c) Perovskite film's thickness as a function of blade-coating speed. (a) Reprinted with permission from [55]. Copyright 2009 American Chemical Society. (b) Reprinted by permission from Macmillan Publishers Ltd: Nature Energy [14], Copyright 2018.

films [55]. The same phenomenon has been found in the meniscus coating of perovskite [14], as shown in figure 4(c). When the coating speed is low, the evaporation regime governs the coating process. The dry film thickness follows a power-law $t \propto v^{-1}$, where the solid particles arrange right below the meniscus. The film thickness decreases as increasing the coating speed due to shorter residence time per unit length, leading to a reduced amount of dried material. Drying at the meniscus position leads to fluid flows in the meniscus which strongly impact film formation. For example, Lin *et al* [56] invented a meniscus-assisted solution printing (MASP) strategy to yield large grain, dense perovskite films. The extremely slow coating speed of 12 μm s^{-1} place their coating process within the evaporation regime (figure 5(a)). Simultaneously, fast solvent evaporation rate at the edge of the meniscus triggered 'coffee ring' effect, transporting perovskite solutes to the contact line, facilitating the growth of micrometer scale grains (figure 5(b)). The solar cells fabricated by this strategy achieved a PCE approaching 20%, benefiting from the low trap density and long carrier lifetimes in the large grain perovskite film. Also, the MASP coated film shows a preferred crystal orientation since the meniscus flows heavily influence the solid film formation at such a low coating speed.

The uniaxially oriented film fabricated by meniscus coating has also been reported in perovskite coating. Van Hest *et al* [57] claimed preferred orientation of the blade coated film at a speed of 2.5–3 m min^{-1}. For solution dissolved by N,N-dimethylformamide (DMF), the coating speed was relatively high, so that evaporation at meniscus area was not fast enough to wholly dry the solvent. However, the authors invented a new solvent by methylamine and acetonitrile, with a very low boiling point and high vapor pressure (figure 5(c)). The fast evaporation of solvent induces an evaporation regime coating process. The Couette flow due to shear force, along with Marangoni and capillary flows drive the growth direction of perovskite film. Consequently, the blade coated film has highly oriented 2D XRD patterns (figure 5(d)) compare to spin-coated film, which consistent with strong periodic XRD peaks that correspond to the (*hk*0) of $MAPbI_3$.

However, not all the reported perovskite films fabricated by the meniscus coating method have a uniaxial orientation. The reason why some reports demonstrate highly oriented films while others do not is due to the coating regime the process employs. Liu *et al* [58] specifically investigated the relationship between meniscus coating speed and film orientation of perovskite films. Results proved that films coated at slow speeds, such as 0.2 mm s^{-1}, exhibit highly aligned morphology. The evaporation within the meniscus region at such slow speed dominates film formation, inducing flow governed orientation. On the other hand, raising speed tremendously changes the solid film morphology, forming large isotropic plate domains. Figures 5(e) and (f) show the apparent morphology difference at various coating speeds. GIWAX data of slow speed coated films confirmed predominant reflection plane is (110) which is parallel to the substrate. Obviously, the preferential orientation originates from the confined nucleation and growth of the moving blade.

Nevertheless, coating film in the Landau–Levich regime is the goal for real production, as faster fabrication is optimal for mass production. Contrary to the slow speed, the faster coating speed of the Landau–Levich regime has a trend of increasing film thickness with coating speed. Wet film forms on the substrate since the coating speed is higher than the solvent drying rate. The separation of wet film spreading and solidification merits the formation of a uniform solid film. However, dewetting of the as-casted wet film before drying can also ruin the solid film uniformity.

3.4. Fate of the wet films after spreading

Unlike the spin-coating process, in which the solvent casting, thinning, and drying all happen at the same place, the meniscus coating in the Landau–Levich regime has spatially separated casting, leveling, and drying processes. The casting process has been comprehensively discussed above. Nevertheless, the fate of the wet layer after casting determines the crystalline film quality. The evaporation of the solvent, nucleation, and growth of solid film play critical roles in solid film formation.

3.4.1. Dewetting. The coating processing of the Landau–Levich regime benefits the healing of irregularities of film thickness originated from the meniscus area. The interval before wet film drying gives time for the liquid film leveling under gravity. However, a spread liquid film can also undergo a dewetting process which ruptures the wet film. Local dewetting can be caused by evaporation, capillary flow, or surface tension gradients. Once the wetting film is sufficiently thin, long-range intermolecular forces can expedite the thinning until cracking occurs. Further, during film solidification, the ruptures can be

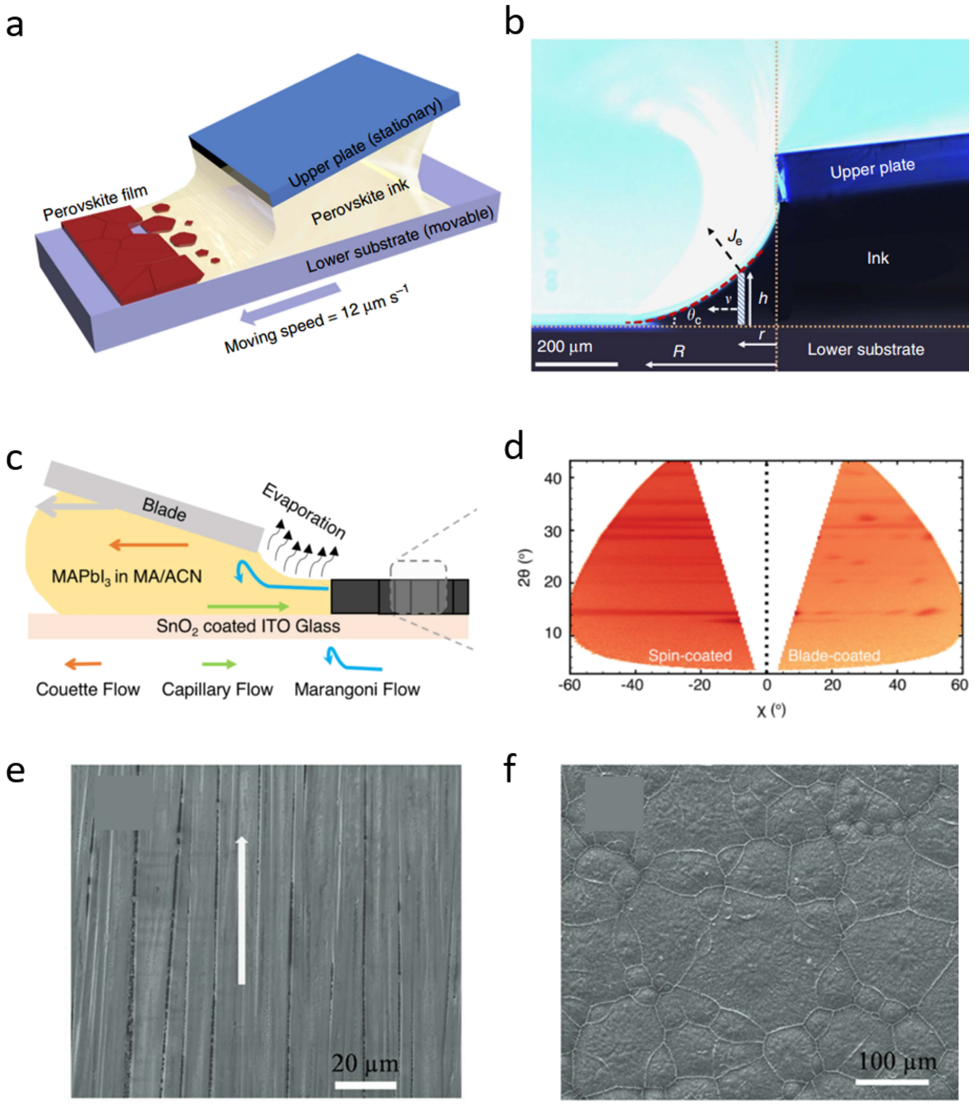

Figure 5. Uniaxial orientation of perovskite films made by blade coating. (a) Schematic diagram of the meniscus-assisted solution coating. (b) Optical micrograph of the side-view meniscus ink confined between a lower flat, movable substrate and an upper stationary plate. (c) Schematic diagram of blade coating at evaporation regime by MA/ACN solvent. (d) 2D-XRD of spin-coated (left) and blade-coated (right) films. (e), (f) Scanning electron microscopy (SEM) of $MAPbI_3$ films blade-coated at different moving speed. Substrate temperature: 100 °C. Coating speed: (e) 0.2 mm s^{-1}, (f) 5 mm s^{-1}. (a) Reproduced from [56]. CC BY 4.0. (b) Reprinted by permission from [58]. Copyright 2018 American Chemical Society. (c) [57] John Wiley & Sons. © 2017 WILEY-VCH Verlag GmbH & Co. KGaA, Weinheim.

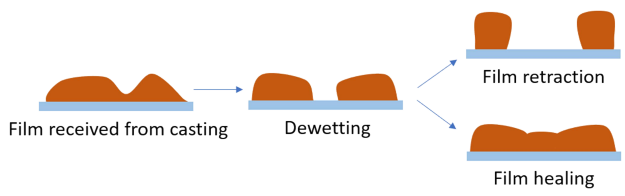

Figure 6. Schematic of dewetting and healing.

enlarged by retraction or healed by the growth of drying domains (figure 6).

DMSO is a commonly used solvent for perovskite precursor solution because it can readily coordinate with lead halide (e.g. PbI_2). The intermediate phase formed by this strong interaction retards the crystallization which encourages the formation of a uniform and dense perovskite film [59]. However, DMSO has high surface tension and a high boiling point of 189 °C. This leads the wet film to contract under surface tension before drying, resulting in holes and gaps in the solid film. To solve this problem, Galagan *et al* [19] mix cosolvent 2-butoxyethanol (2BE) with DMSO to R2R slot-die coat methylammonium lead iodide and other mixed cation and mixed halide perovskites. 2BE has a low boiling point and small surface tension. It not only reduces the net surface tension, improving the wettability of the wet layer but also increases the evaporation rate, leading to fast drying and mitigating the dewetting phenomenon. Besides, the authors further accelerate solvent evaporation rate by setting a faster

temperature ramp-up after coating. Through these strategies, the solidification of the wet layer has been well controlled. A compact plate-like perovskite film fabricated by R2R slot-die coating on ITO-PET achieved highest PCE of 13.5%.

We demonstrated that surfactant is another strategy to avoid dewetting of the blade-coated wet film [14]. Usually the hydrophobic properties of hole transportation material poly (bis(4-phenyl)) (2,4,6-trimethylphenyl) amine (PTAA) make it challenging to form compact perovskite layer. However, the surfactants in perovskite solution effectively modified the ink/substrate interface and improved the affinity of perovskite solution to substrates. In this way, the surfactant facilitates the formation of fully coverage perovskite layer on the hydrophobic PTAA by blade coating.

After forming a uniform, fully covered wetting layer, several phenomena affect the evolution of the film, including solvent evaporation, thinning of wetting layer, phase transition, and solidification. Each of the processes can critically influence the morphology and electrical properties of final crystalline perovskite film.

3.4.2. Drying and crystallization. Although researchers have long known that controlling the solidification process is an essential key in achieving a high-quality perovskite film, it is only recently that researchers used *in situ* characterization techniques to elucidate the process in the transition from precursor solution to solid film while spin-coating or meniscus coating. *In situ* characterizations unveil that unlike polymer semiconductors, perovskite undergoes a unique phase transition during the solution coating process. The so-called intermediate phase which forms because of the coordination of solvent and lead halide plays a critical role in film formation.

In situ timeresolved grazing-incidence wideangle x-ray scattering (GIWAXS) is a powerful tool to investigate the phase behavior in the film coating process. Amassian *et al* [60] first observed the phase transition in spin-coating $MAPbI_3$ in DMF. A highly ordered intermediate phase out of the disordered precursor formed 20 s after casting, which shows three intense peaks at low scattering vector q values. The phase is stable without additional treatment. The morphology of such films exhibits a needle-like structure, which stems mainly from the preferred orientation of intermediate phase crystal. The ordered intermediate solvate phase and needle-like morphology have also been observed in films blade coated by the same ink formulation at room temperate [61]. However, heating the substrate during blade-coating has been found to significantly alter the phase transition process. Substrate temperature higher than 100 °C can completely circumvent the solvate phase, which mainly due to the fast removal of the solvent in the as-casted wet film. GIWAX shows a direct transformation from disordered colloids to perovskite phase. A compact film with large domains rather than needle-like morphology has been formed. Not surprisingly, the PCE has improved because of the compact morphology by high-temperature blade coating. Recently, Liu *et al* [62] elucidated the identical key point for forming a high-quality perovskite film by spin-coating and blade-coating: suppressing intermediate phase over-crystallization, regardless of coating temperature. Intermediate phase is widely accepted as a pivotal to growing large perovskite crystals [63]. However, the over-crystallization of intermediate phase distorts the morphology to textured, incomplete coverage. As a consequence, the anti-solvent dripping method must be controlled precisely due to the narrow operation window of supersaturating solvent without solvate phase over-crystallization (figure 7(a)). In the hot substrate scenario, the high temperature helps evaporate solvent immediately after coating. The extremely fast evaporation directly transits disordered sol-gel to perovskite phase, circumventing the intermediate phase (figure 7(c)).

So far, several strategies have been established to realize controllable solvent removal rate, including anti-solvent, hot substrate, and gas quenching. The basic ideas are all based on suppressing over-crystallization of intermediate phase or even completely avoiding it.

3.4.2.1. Antisolvent. As mentioned above, anti-solvent dripping has been widely used in spin-coating to produce high-quality perovskite films. However, the common dripping process is challenging to implement with the meniscus coating. However, instead of dripping, Zhu *et al* incorporated blade coating with anti-solvent bathing method [64, 65] (figure 8(a)). Unfortunately, the timescale of transferring the as-casted wet film to the solvent bath is much longer than the intermediate phase formation time. As a consequence, bad morphology appears even with the anti-solvent applied. On the other hand, additives such as methylammonium chloride (MACl) are commonly used to control perovskite morphology [66, 67]. The authors take advantage of MACl to prolong the operation window for antisolvent treatment. An 8 min wet-film stage can be achieved by adding excess MACl to the $MAPbI_3$ precursor solution, which decouples the precursor film casting and perovskite formation, enabling the antisolvent extraction. The devices made by such strategy achieved PCE of 18.55% with 0.12 cm^2 area, and 13.3% active-area efficiency of a 12.6 cm^2 module.

3.4.2.2. Hot substrate. Heating substrate is a simple way to facilitate solvent evaporation (figure 8(b)). It has been widely used ever since the early stages of study on meniscus coating perovskite [13–16, 68, 69]. Boiling points of commonly used solvents DMF, DMSO, GBL, NMP are 152 °C–154 °C, 189 °C, 206 °C and 202 °C–204 °C respectively. To remove these solvents completely and effectively, the substrate must be kept at a temperature close to the solvent's boiling point. Greater than half of all works reviewed used the hot substrate strategy to meniscus coat perovskite (table 2). The highest device efficiencies based on meniscus coated perovskite also implement heating of the substrate during coating. Recently, we incorporate bilateral alkylamine (BAA) as a multifunctional additive in perovskite precursor for blade coating with 150 °C substrate temperature. The optimized device achieved a champion PCE of 21.7% with 21.5% stabilized output [70]. Moreover, we also showed the

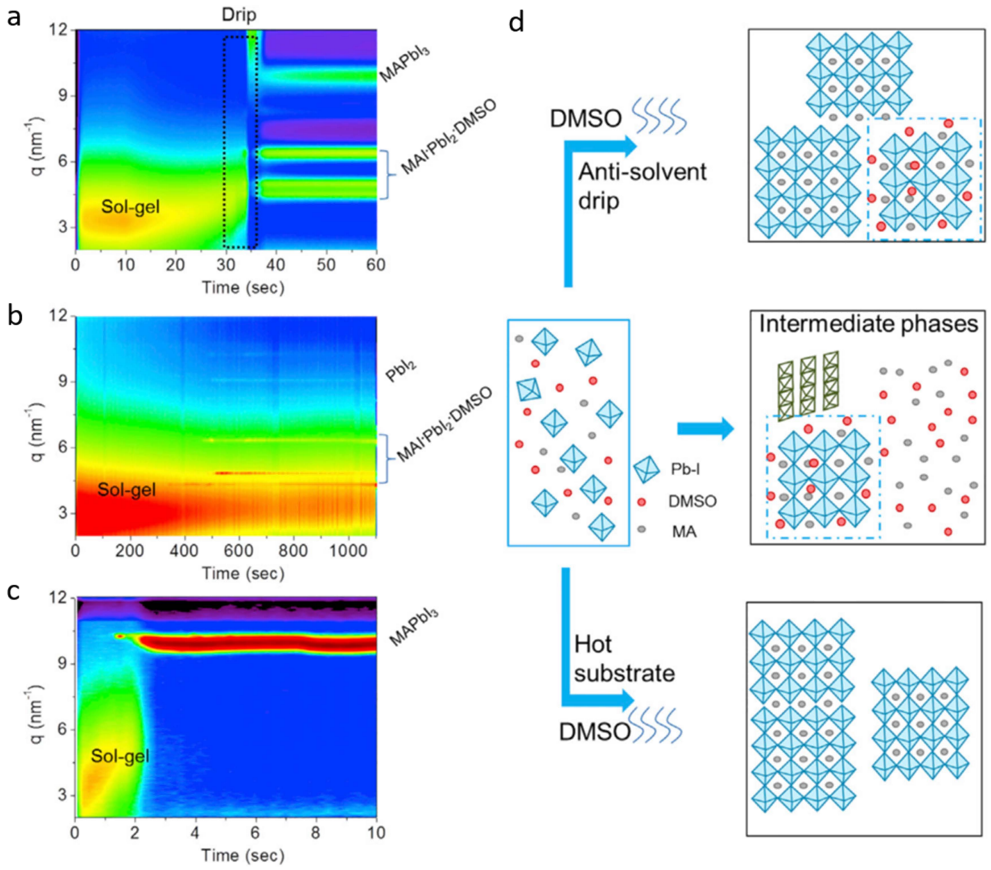

Figure 7. *In situ* GIWAXS measurements of $MAPbI_3$ for different fabrication conditions. (a) DMSO: GBL-blade-25 °C with the anti-solvent drip. (b) DMSO: GBL-blade-25 °C. (c) DMSO: GBL-blade-150 °C. (d) Schematic models of the $MAPbI_3$ structural evolution for the three cases. Reprinted from [62], Copyright 2018, with permission from Elsevier.

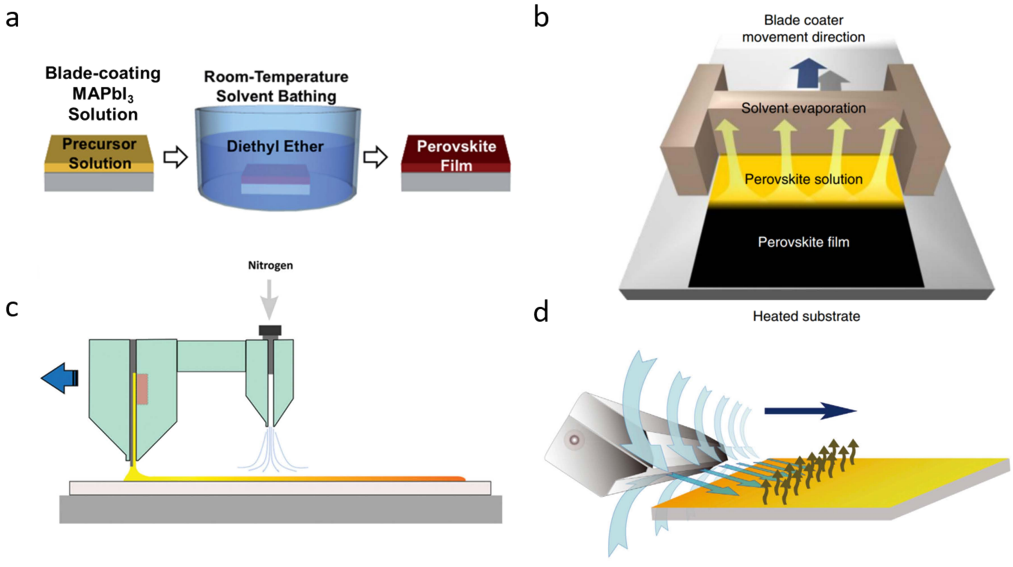

Figure 8. Schematic illustrations of solvent removal strategies. (a) Antisolvent bathing of blade-coated perovskite thin film. (b) Blade coating on hot substrate. (c) Slot-die coating with gas-quenching. (d) Air-blading to dry perovskite wet film. (a) Reproduced from [65] with permission of The Royal Society of Chemistry. (b) Reprinted by permission from Macmillan Publishers Ltd: Nature Energy [14], Copyright 2018. (c) [20] John Wiley & Sons. © 2015 WILEY-VCH Verlag GmbH & Co. KGaA, Weinheim. (d) Reprinted from [74], Copyright 2018, with permission from Elsevier.

Table 2. Summary of PCE of meniscus coating devices and their solvent removal strategies.

Coating method	Perovskite	Solvent	Solvent removal strategy	State-of-art efficiency (%)	References
Blade coating	$CH_3NH_3PbI_{3-x}Cl_x$	DMF	RT evaporation	12.21	[84]
	$CH_3NH_3PbI_{3-x}Cl_x$	DMF	Post annealing	10.44	[68]
	$MAPbI_3$	MA/ACN	Low boiling point solvent	19.6	[57]
	$MAPbI_3$	NMP/DMF	Anti-solvent bathing	18.55	[64]
	$MAPbI_3$	DMF	Hot substrate	15.1	[16]
	$MAPbI_3$	DMF	Hot substrate	12.11	[69]
	$FA_{0.4}MA_{0.6}PbI_3$	DMF	Hot substrate	18.3	[15]
	$MA_{0.6}FA_{0.38}Cs_{0.02}PbI_{2.975}Br_{0.025}$	DMF	Hot substrate	19.5	[82]
	$FA_{0.85}MA_{0.15}PbI_{2.55}Br_{0.45}$	DMSO	Hot substrate	20.05	[56]
	$MAPbI_3$	DMF	Hot substrate	20.2	[13]
	$MAPbI_3$	DMF	Hot substrate	17.54	[61]
	$MAPbI_3$	DMF	Hot substrate	20.3 (14.6% of 57.2 cm^2 module)	[14]
	$MAPbI_3$	DMF	Hot substrate	21.70	[70]
	$MAPbI_3$	DMF/DMSO	Gas quenching	19.3	[74]
	$Cs_{0.05}FA_{0.81}MA_{0.14}PbI_{2.55}Br_{0.45}$	DMF/DMSO	Gas quenching	20.26	[75]
Slot-die coating	$MAPbI_3$	DMF	Post annealing	16.8 (11.2% of 149.5 cm^2 module)	[17]
	$Cs_{0.15}FA_{0.85}PbI_{2.85}Br_{0.15}$	DMSO	Post annealing	13.5	[19]
	$MAPbI_3$	MA/ACN	Low boiling point solvent	17.3	[57]
	$MAPbI_3$	NMP/DMF	Anti-solvent bathing	18	[85]
	$CH_3NH_3PbI_{3-x}Cl_x$	DMF	Hot substrate	2.39	[86]
	$MAPbI_3$	DMF	Gas quenching	11.96	[20]
	$MAPbI_3$	DMF	Hot substrate + gas quenching	15.57	[87]
	$CH_3NH_3PbI_{3-x}Cl_x$	DMF	Hot substrate + gas quenching	9.2	[72]
	$MAPbI_3$	DMF	Hot substrate + gas quenching	11.4	[73]

capability of hot substrate blade coating strategy on making perovskite modules. By combining the surfactant additive as mentioned before, we demonstrated perovskite modules of up to 14.6% efficiency for a 57.2 cm^2 aperture area [14].

3.4.2.3. Gas quenching. The gas quenching method is believed to have good reproducibility as it avoids using chemicals and is a low-temperature process [71]. The flowing gas takes away the solvent from the as-coated wet layer on substrates, leaving perovskite materials to form the solid film (figure 8(c)). Many excellent results based on this method were reported in spin coating techniques; meniscus coating can also take advantage of this strategy. Vak *et al* [20] slot-die coat perovskite film by two steps method. The N_2 gas was introduced to accelerate the solvent evaporation during slot-die coating the PbI_2 layer, forming a pinhole-free uniform film. After that, MAI was employed by slot-die system to convert PbI_2 to perovskite. A PCE of 10.14% was demonstrated, which is the highest efficiency of a fully slot-die coated PSC. Other works integrate the gas-quenching with a hot substrate to facilitate solvent evaporation. A heater was equipped on the slot-die machine to heat the substrate. A gas blower was housed behind the slot die-heat to flow N_2 above the film surface. Benefitting from the gas flowing, the substrate temperature must not be as high without the gas quenching. Temperatures ranging from 45 °C to 65 °C were found to be the optimized parameters [20, 72, 73]. The best PSCs fabricated by such method achieved PCE of 15.57% [72]. Moreover, gas quenching can be facilely employed without doctor blading. Hu *et al* [74] blew N_2 gas on a wet perovskite film directly (figure 8(d)). The gas can blow away the solvent efficiently due to the low moving speed (5 mm s^{-1}) of the gas knife. The devices made by fully air-blading method achieved PCE of 20.8% for 0.09 cm^2 and 19.12% for 1.0 cm^2. While this review is preparing, Li *et al* combined the gas quenching and blade coating, achieving a hysteresis-free PSCs with PCE of 20.26% for 0.06 cm^2 [75]. The air knife was installed in a way that laminar nitrogen blows in a horizontal direction. This setup not only provides reproducible processes but also enables *in situ* measurements on the film's drying and crystallization.

3.5. Meniscus coating mix cation/anion perovskite

Up to now, most devices fabricated by the meniscus coating method still work on $MAPbI_3$, as a single composition is easy to control. However, mixed cation and anion perovskites have

been well known to have numerous advantages that single component perovskites cannot reach, including higher performance, increased stability, enabling band gap tuning, enhanced charge carrier transport, etc [76].

Formamidinium (FA) in $MAPbI_3$ can reduce the bandgap, enabling the devices to approach the optimization bandgap of Shockley–Queisier limit [77]. However, FA perovskite is thermodynamically stable in a δ phase at room temperature, which needs enough energy to overcome the phase transition barrier to perovskite phase. Inspired by the hot substrate blade coating, which enables heating the substrate and blading precursor solution simultaneously [15], we successfully made FA and MA mixed perovskite by the blade coating method. The high-temperature substrate not only helps accelerate solvent evaporation but also overcome the energy barrier of δ phase to α phase. Mixed cation perovskite $FA_{0.4}MA_{0.6}PbI_3$ reached a bandgap of 1.55 eV. The champion cell yielded a PCE of 18.3%, which is higher than the $MAPbI_3$ devices fabricated by the same process. Cesium is another widely used A site element. Cs ion was designed to substitute part of organic ions to improve thermal and structural stability [78]. Fortunately, Cs ions in combination with MA were found to facilitate crystallization of precursor solution to solid perovskite phase at room temperature [79]. As a result, it is possible to fabricate triple cation perovskite by the meniscus coating method without heating the substrate. Furthermore, Cs interacts strongly with $[PbI_6]^{4-}$ which replaces the intercalated DMSO, reducing the concentration of intermediate phase and promoting rapid crystallinity.

At the halide site, chloride was first introduced in $MAPbI_3$ to obtain outstanding PV performance. However, comprehensive studies revealed that the big halogen ionic radii difference hindered the incorporation of Cl from forming perovskite phase [80]. Instead, the real role of the Cl ions is as a dopant that influences the crystallization process. This property has been used in meniscus coating as mentioned previously [64]. Contrary to chloride, bromide can alloy with iodide, increasing perovskite bandgap up to 2.3 eV [81]. We also demonstrated that incorporating Cs and Br in perovskite precursor solution can reduce the required film formation temperature for blade coating [82]. A blading temperature of 120 °C was used to form a high-quality film of $MA_{0.6}FA_{0.38}Cs_{0.02}PbI_{2.975}Br_{0.025}$ perovskite, compared to 150 °C for $MAPbI_3$ composition. Such mix cation and halide film achieved stabilized PCE of 19.3% with less than 10% degradation after storage for one month.

Although mixed tin-lead perovskite is another hot topic in perovskite research—due to potential in tandem solar cell applications—few reports have studied meniscus coating of tin perovskite films. One likely reason is due to the fast nucleation and crystal growth rate of tin perovskite [83], leading to uncontrollable crystallization, especially in meniscus coating.

4. Summary and outlook

The advancement of coating methods and morphology control strategies in perovskite film fabrication will undoubtedly bring us into a bright future of PV applications. It is clear that thoroughly understanding and control of perovskite solution spreading, drying, and crystallization during meniscus coating is essential to achieving device high-performance. Notably, *in situ* characterization of phase transition and morphology evolution has provided valuable insights into the dynamics of film formation. More comprehensive studies will further unveil the mechanisms of meniscus coating of perovskite films. Moreover, since meniscus coating is compatible with an R2R processing system, fundamental studies will guide the way to large scale, high-speed production. Nevertheless, numerous challenges remain. Comprehensive understanding of meniscus coating mixed cation/anion perovskite films must be attained. Lack of work in this arena see it lagging behind its spin-coating counterpart. Intensive studies of the film evolution in mixed cation/anion perovskite can provide direction to achieving high-quality films. Though the main issue covered in this review is meniscus coating the perovskite active layer, mass production of PSCs requires scalable manufacturing of each layer of the device stack. Polymer carrier transportation layers are the simplest challenge to overcome due to extensive study. The Achilles' heel is the scalable fabrication of the top electrode. The carbon electrode is a promising candidate and is more suitable to meniscus coating method than spin-coating. At this point, meniscus coating is the most promising technique to realize fully scalable fabrication of PSCs.

Acknowledgments

This work was supported by Office of Naval Research under award N00014-17-1-2619. Certain images in this publication have been obtained by the author(s) from the Wikimedia website, where they were made available under a Creative Commons licence or stated to be in the public domain. Please see individual figure captions in this publication for details. To the extent that the law allows, IOP Publishing disclaim any liability that any person may suffer as a result of accessing, using or forwarding the image(s). Any reuse rights should be checked and permission should be sought if necessary from Wikimedia and/or the copyright owner (as appropriate) before using or forwarding the image.

ORCID iDs

Xuezeng Dai https://orcid.org/0000-0002-5544-590X
Jinsong Huang https://orcid.org/0000-0002-0509-8778

References

[1] Global Market Outlook 2019 2018–2022 http://solarpowereurope.org/global-market-outlook-2018-2022/ (Accessed: April 2019)
[2] Annual Energy Outlook 2019 https://eia.gov/outlooks/aeo/pdf/electricity_generation.pdf (Accessed: April 2019)

[3] Huang J, Yuan Y, Shao Y and Yan Y 2017 Understanding the physical properties of hybrid perovskites for photovoltaic applications *Nat. Rev. Mater.* **2** 17042

[4] Dong Q, Fang Y, Shao Y, Mulligan P, Qiu J, Cao L and Huang J 2015 Electron–hole diffusion lengths >175 μm in solution grown $CH_3NH_3PbI_3$ single crystals *Science* **347** 967–70

[5] Xiao Z, Yuan Y, Shao Y, Wang Q, Dong Q, Bi C, Sharma P, Gruverman A and Huang J 2015 Giant switchable photovoltaic effect in organometal trihalide perovskite devices *Nat. Mater.* **14** 193

[6] Wei H, Fang Y, Mulligan P, Chuirazzi W, Fang H-H, Wang C, Ecker B R, Gao Y, Loi M A and Cao L 2016 Sensitive x-ray detectors made of methylammonium lead tribromide perovskite single crystals *Nat. Photonics* **10** 333

[7] Stranks S D, Eperon G E, Grancini G, Menelaou C, Alcocer M J, Leijtens T, Herz L M, Petrozza A and Snaith H J 2013 Electron–hole diffusion lengths exceeding 1 micrometer in an organometal trihalide perovskite absorber *Science* **342** 341–4

[8] NREL PV Research Cell Record Efficiency Chart 2019 https://nrel.gov/pv/cell-efficiency.html (Accessed: April 2019)

[9] Cai M, Wu Y, Chen H, Yang X, Qiang Y and Han L 2017 Cost-performance analysis of perovskite solar modules *Adv. Sci.* **4** 1600269

[10] Song Z, McElvany C L, Phillips A B, Celik I, Krantz P W, Watthage S C, Liyanage G K, Apul D and Heben M J 2017 A technoeconomic analysis of perovskite solar module manufacturing with low-cost materials and techniques *Energy Environ. Sci.* **10** 1297–305

[11] Turkevych I *et al* 2019 Strategic advantages of reactive polyiodide melts for scalable perovskite photovoltaics *Nat. Nanotechnol.* **14** 57–63

[12] Oxford 2019 PV perovskite solar cell achieves 28% efficiency https://oxfordpv.com/news/oxford-pv-perovskite-solar-cell-achieves-28-efficiency (Accessed: April 2019)

[13] Wu W-Q, Wang Q, Fang Y, Shao Y, Tang S, Deng Y, Lu H, Liu Y, Li T and Yang Z 2018 Molecular doping enabled scalable blading of efficient hole-transport-layer-free perovskite solar cells *Nat. Commun.* **9** 1625

[14] Deng Y, Zheng X, Bai Y, Wang Q, Zhao J and Huang J 2018 Surfactant-controlled ink drying enables high-speed deposition of perovskite films for efficient photovoltaic modules *Nat. Energy* **3** 560–6

[15] Deng Y, Dong Q, Bi C, Yuan Y and Huang J 2016 Air-stable, efficient mixed-cation perovskite solar cells with Cu electrode by scalable fabrication of active layer *Adv. Energy Mater.* **6** 1600372

[16] Deng Y, Peng E, Shao Y, Xiao Z, Dong Q and Huang J 2015 Scalable fabrication of efficient organolead trihalide perovskite solar cells with doctor-bladed active layers *Energy Environ. Sci.* **8** 1544–50

[17] Di Giacomo F *et al* 2018 Up-scalable sheet-to-sheet production of high efficiency perovskite module and solar cells on 6-in. substrate using slot die coating *Solar Energy Mater. Solar Cells* **181** 53–9

[18] Hu Q, Zhao L, Wu J, Gao K, Luo D, Jiang Y, Zhang Z, Zhu C, Schaible E and Hexemer A 2017 *In situ* dynamic observations of perovskite crystallisation and microstructure evolution intermediated from [PbI 6] 4− cage nanoparticles *Nat. Commun.* **8** 15688

[19] Galagan Y, Di Giacomo F, Gorter H, Kirchner G, de Vries I, Andriessen R and Groen P 2018 Roll-to-roll slot die coated perovskite for efficient flexible solar cells *Adv. Energy Mater.* **8** 1801935

[20] Hwang K, Jung Y S, Heo Y J, Scholes F H, Watkins S E, Subbiah J, Jones D J, Kim D Y and Vak D 2015 Toward large scale roll-to-roll production of fully printed perovskite solar cells *Adv. Mater.* **27** 1241–7

[21] Barrows A T, Pearson A J, Kwak C K, Dunbar A D, Buckley A R, Lidzey D G and Science E 2014 Efficient planar heterojunction mixed-halide perovskite solar cells deposited via spray-deposition *Energy Environ. Sci.* **7** 2944–50

[22] Bag S, Deneault J R and Durstock M F 2017 Aerosol-jet-assisted thin-film growth of $CH_3NH_3PbI_3$ perovskites—a means to achieve high quality defect-free films for efficient solar cells *Adv. Energy Mater.* **7** 1701151

[23] Kim J, Yun J S, Cho Y, Lee D S, Wilkinson B, Soufiani A M, Deng X, Zheng J, Shi A and Lim S 2017 Overcoming the challenges of large-area high-efficiency perovskite solar cells *ACS Energy Lett.* **2** 1978–84

[24] Mathies F, Abzieher T, Hochstuhl A, Glaser K, Colsmann A, Paetzold U W, Hernandez-Sosa G, Lemmer U and Quintilla A 2016 Multipass inkjet printed planar methylammonium lead iodide perovskite solar cells *J. Mater. Chem.* A **4** 19207–13

[25] Li S-G, Jiang K-J, Su M-J, Cui X-P, Huang J-H, Zhang Q-Q, Zhou X-Q, Yang L-M and Song Y-L 2015 Inkjet printing of $CH_3NH_3PbI_3$ on a mesoscopic TiO_2 film for highly efficient perovskite solar cells *J. Mater. Chem.* A **3** 9092–7

[26] Bag M, Jiang Z, Renna L A, Jeong S P, Rotello V M and Venkataraman D 2016 Rapid combinatorial screening of inkjet-printed alkyl-ammonium cations in perovskite solar cells *Mater. Lett.* **164** 472–5

[27] Solaronix Achieves Major Breakthrough Toward Perovskite Solar Cell Industrialization https://solaronix.com/news/solaronix-achieves-major-breakthrough-toward-perovskite-solar-cell-industrialization/ (Accessed: April 2019)

[28] Li Z, Klein T R, Kim D H, Yang M, Berry J J, van Hest M F and Zhu K 2018 Scalable fabrication of perovskite solar cells *Nat. Rev. Mater.* **3** 18017

[29] NEDO and Toshiba Develops World's Largest Film-based Perovskite Photovoltaic Module 703 cm^2 Module Achieves 11.7% Power Conversion Efficiency https://toshiba.co.jp/rdc/rd/detail_e/e1806_03.html (Accessed: April 2019)

[30] Green M A, Hishikawa Y, Dunlop E D, Levi D H, Hohl-Ebinger J, Yoshita M and Ho-Baillie A W Y 2019 Solar cell efficiency tables (version 53) *Prog. Photovolt. Res. Appl.* **27** 3–12

[31] Bi C, Wang Q, Shao Y, Yuan Y, Xiao Z and Huang J 2015 Non-wetting surface-driven high-aspect-ratio crystalline grain growth for efficient hybrid perovskite solar cells *Nat. Commun.* **6** 7747

[32] Jung E H, Jeon N J, Park E Y, Moon C S, Shin T J, Yang T-Y, Noh J H and Seo J 2019 Efficient, stable and scalable perovskite solar cells using poly (3-hexylthiophene) *Nature* **567** 511

[33] Jiang Q, Zhao Y, Zhang X, Yang X, Chen Y, Chu Z, Ye Q, Li X, Yin Z and You J 2019 Surface passivation of perovskite film for efficient solar cells *Nat. Photonics* **13** 460–6

[34] Reese M O, Glynn S, Kempe M D, McGott D L, Dabney M S, Barnes T M, Booth S, Feldman D and Haegel N M 2018 Increasing markets and decreasing package weight for high-specific-power photovoltaics *Nat. Energy* **3** 1002

[35] Ten Elshof J E 2015 4—chemical solution deposition techniques for epitaxial growth of complex oxides *Epitaxial Growth of Complex Metal Oxides* ed G Koster *et al* (Cambridge: Woodhead Publishing) pp 69–93

[36] Twiname E and Mistler R 2001 Tape casting and lamination *Encyclopedia of Materials: Science and Technology* 2nd edn pp 9083–8

[37] Kistler S F and Schweizer P M 1997 *Liquid Film Coating: Scientific Principles and Their Technological Implications* (Berlin: Springer) (https://doi.org/10.1007/978-94-011-5342-3)

[38] Blake T D 2006 The physics of moving wetting lines *J. Colloid Interface Sci.* **299** 1–13

[39] Kistler S F 1993 *Wettability* ed J C Berg (New York: Marcel Dekker)

[40] Loeb G I and Schrader M E 2013 *Modern Approaches to Wettability: Theory and Applications* (New York: Springer) (https://doi.org/10.1007/978-1-4899-1176-6)

[41] Young T 1805 III. An essay on the cohesion of fluids *Phil. Trans. Royal Soc. London* **95** 65

[42] Wenzel R N 1949 Surface roughness and contact angle *J. Phys. Colloid Chem.* **53** 1466–7

[43] Cassie A B D and Baxter S 1944 Wettability of porous surfaces *Trans. Faraday Soc.* **40** 546–51

[44] Liu C-Y, Carvalho M S and Kumar S J 2017 Mechanisms of dynamic wetting failure in the presence of soluble surfactants *J. Fluid Mech.* **825** 677–703

[45] Girard F, Antoni M, Faure S and Steinchen A 2006 Evaporation and Marangoni driven convection in small heated water droplets *Langmuir* **22** 11085–91

[46] Pelcé P and Libchaber A 2012 *Dynamics of Curved Fronts* (Amsterdam: Elsevier) (https://doi.org/10.1016/C2009-0-22180-5)

[47] Washburn E W 1921 The dynamics of capillary flow *Phys. Rev.* **17** 273–83

[48] Lun C, Savage S B, Jeffrey D and Chepurniy N J 1984 Kinetic theories for granular flow: inelastic particles in Couette flow and slightly inelastic particles in a general flowfield *J. Fluid Mech.* **140** 223–56

[49] Levich V and Krylov V 1969 Surface-tension-driven phenomena *Ann. Rev. Fluid Mech.* **1** 293–316

[50] Zhang Z, Peng B, Ji X, Pei K and Chan P K L 2017 Marangoni-effect-assisted bar-coating method for high-quality organic crystals with compressive and tensile strains *Adv. Funct. Mater.* **27** 1703443

[51] Deegan R D, Bakajin O, Dupont T F, Huber G, Nagel S R and Witten T A 1997 Capillary flow as the cause of ring stains from dried liquid drops *Nature* **389** 827

[52] Deegan R D, Bakajin O, Dupont T F, Huber G, Nagel S R and Witten T A 2000 Contact line deposits in an evaporating drop *Phys. Rev.* E **62** 756

[53] Ishihara H, Chen W, Chen Y C, Sarang S, De Marco N, Lin O, Ghosh S and Tung V I 2016 Electrohydrodynamically assisted deposition of efficient perovskite photovoltaics *Adv. Mater. Interfaces* **3** 1500762

[54] Landau L and Levich B 1988 Dragging of a liquid by a moving plate *Dynamics of Curved Fronts* ed P Pelcé (San Diego, CA: Academic) pp 141–53

[55] Le Berre M, Chen Y and Baigl D 2009 From convective assembly to Landau–Levich deposition of multilayered phospholipid films of controlled thickness *Langmuir* **25** 2554–7

[56] He M, Li B, Cui X, Jiang B, He Y, Chen Y, O'Neil D, Szymanski P, Ei-Sayed M A and Huang J 2017 Meniscus-assisted solution printing of large-grained perovskite films for high-efficiency solar cells *Nat. Commun.* **8** 16045

[57] Dou B, Whitaker J B, Bruening K, Moore D T, Wheeler L M, Ryter J, Breslin N J, Berry J J, Garner S M and Barnes F S 2018 Roll-to-roll printing of perovskite solar cells *ACS Energy Lett.* **3** 2558–65

[58] Li J *et al* 2017 Solution coating of superior large-area flexible perovskite thin films with controlled crystal packing *Adv. Opt. Mater.* **5** 1700102

[59] Ahn N, Son D-Y, Jang I-H, Kang S M, Choi M and Park N-G 2015 Highly reproducible perovskite solar cells with average efficiency of 18.3% and best efficiency of 19.7% fabricated via lewis base adduct of lead(II) iodide *J. Am. Chem. Soc.* **137** 8696–9

[60] Munir R *et al* 2017 Hybrid perovskite thin-film photovoltaics: *in situ* diagnostics and importance of the precursor solvate phases *Adv. Mater.* **29** 1604113

[61] Zhong Y, Munir R, Li J, Tang M-C, Niazi M R, Smilgies D-M, Zhao K and Amassian A 2018 Blade-coated hybrid perovskite solar cells with efficiency > 17%: an *in situ* investigation *ACS Energy Lett.* **3** 1078–85

[62] Li J, Munir R, Fan Y, Niu T, Liu Y, Zhong Y, Yang Z, Tian Y, Liu B and Sun J 2018 Phase transition control for high-performance blade-coated perovskite solar cells *Joule* **2** 1313–30

[63] Bai Y, Xiao S, Hu C, Zhang T, Meng X, Li Q, Yang Y, Wong K S, Chen H and Yang S 2017 A pure and stable intermediate phase is key to growing aligned and vertically monolithic perovskite crystals for efficient PIN planar perovskite solar cells with high processibility and stability *Nano Energy* **34** 58–68

[64] Yang M *et al* 2017 Perovskite ink with wide processing window for scalable high-efficiency solar cells *Nat. Energy* **2** 17038

[65] Zhou Y, Yang M, Wu W, Vasiliev A L, Zhu K and Padture N P 2015 Room-temperature crystallization of hybrid-perovskite thin films via solvent–solvent extraction for high-performance solar cells *J. Mater. Chem.* A **3** 8178–84

[66] Zhao Y and Zhu K 2014 CH_3NH_3Cl-assisted one-step solution growth of $CH_3NH_3PbI_3$: structure, charge-carrier dynamics, and photovoltaic properties of perovskite solar cells *J. Phys. Chem.* C **118** 9412–8

[67] Yan K, Long M, Zhang T, Wei Z, Chen H, Yang S and Xu J 2015 Hybrid halide perovskite solar cell precursors: colloidal chemistry and coordination engineering behind device processing for high efficiency *J. Am. Chem. Soc.* **137** 4460–8

[68] Yang Z, Chueh C-C, Zuo F, Kim J H, Liang P-W and Jen A K Y 2015 High-performance fully printable perovskite solar cells via blade-coating technique under the ambient condition *Adv. Energy Mater.* **5** 1500328

[69] Deng Y, Wang Q, Yuan Y and Huang J 2015 Vividly colorful hybrid perovskite solar cells by doctor-blade coating with perovskite photonic nanostructures *Mater. Horiz.* **2** 578–83

[70] Wu W-Q *et al* 2019 Bilateral alkylamine for suppressing charge recombination and improving stability in blade-coated perovskite solar cells *Sci. Adv.* **5** eaav8925

[71] Huang F *et al* 2014 Gas-assisted preparation of lead iodide perovskite films consisting of a monolayer of single crystalline grains for high efficiency planar solar cells *Nano Energy* **10** 10–8

[72] Cotella G, Baker J, Worsley D, De Rossi F, Pleydell-Pearce C, Carnie M and Watson T 2017 One-step deposition by slot-die coating of mixed lead halide perovskite for photovoltaic applications *Sol. Energy Mater. Sol. Cells* **159** 362–9

[73] Lee D, Jung Y-S, Heo Y-J, Lee S, Hwang K, Jeon Y-J, Kim J-E, Park J, Jung G Y and Kim D-Y 2018 Slot-die coated perovskite films using mixed lead precursors for highly reproducible and large-area solar cells *ACS Appl. Mater. Interfaces* **10** 16133–9

[74] Ding J, Han Q, Ge Q-Q, Xue D-J, Ma J-Y, Zhao B-Y, Chen Y-X, Liu J, Mitzi D B and Hu J-S 2018 Fully air-bladed high-efficiency perovskite photovoltaics *Joule* **3** 402–16

[75] Hu H, Ren Z, Fong P W, Qin M, Liu D, Lei D, Lu X and Li G 2019 Room-temperature meniscus coating of >20% perovskite solar cells: a film formation mechanism investigation *Adv. Funct. Mater.* **29** 1900092

[76] Ono L K, Juarez-Perez E J and Qi Y 2017 Progress on perovskite materials and solar cells with mixed cations and halide anions *ACS Appl. Mater. Interfaces* **9** 30197–246

[77] Shockley W and Queisser H J 1961 Detailed balance limit of efficiency of p-n junction solar cells *J. Appl. Phys.* **32** 510–9

[78] Saliba M *et al* 2016 Cesium-containing triple cation perovskite solar cells: improved stability, reproducibility and high efficiency *Energy Environ. Sci.* **9** 1989–97

[79] Matsui T, Seo J Y, Saliba M, Zakeeruddin S M and Grätzel M 2017 Room-temperature formation of highly crystalline multication perovskites for efficient, low-cost solar cells *Adv. Mater.* **29** 1606258

[80] Colella S, Mosconi E, Fedeli P, Listorti A, Gazza F, Orlandi F, Ferro P, Besagni T, Rizzo A and Calestani G 2013 $MAPbI_{3-x}Cl_x$ mixed halide perovskite for hybrid solar cells: the role of chloride as dopant on the transport and structural properties *Chem. Mater.* **25** 4613–8

[81] Noh J H, Im S H, Heo J H, Mandal T N and Seok S I 2013 Chemical management for colorful, efficient, and stable inorganic–organic hybrid nanostructured solar cells *Nano Lett.* **13** 1764–9

[82] Tang S, Deng Y, Zheng X, Bai Y, Fang Y, Dong Q, Wei H and Huang J 2017 Composition engineering in doctor-blading of perovskite solar cells *Adv. Energy Mater.* **7** 1700302

[83] Konstantakou M and Stergiopoulos T 2017 A critical review on tin halide perovskite solar cells *J. Mater. Chem.* A **5** 11518–49

[84] Kim J H, Williams S T, Cho N, Chueh C-C and Jen A K-Y 2015 Enhanced environmental stability of planar heterojunction perovskite solar cells based on blade-coating *Adv. Energy Mater.* **5** 1401229

[85] Whitaker J B, Kim D H, Larson B W, Zhang F, Berry J J, van Hest M F and Zhu K 2018 Fuels, Scalable slot-die coating of high performance perovskite solar cells *Sust. Energy Fuels* **2** 2442–9

[86] Ciro J, Mejía-Escobar M A and Jaramillo F 2017 Slot-die processing of flexible perovskite solar cells in ambient conditions *Sol. Energy* **150** 570–6

[87] Zuo C, Vak D, Angmo D, Ding L and Gao M 2018 One-step roll-to-roll air processed high efficiency perovskite solar cells *Nano Energy* **46** 185–92